RECONSTRUCTION OF FRACTURE PROCESS OF SPHEROIDAL GRAPHITE CAST IRON BY ANALYZING THE CONFOCAL SCANNING LASER MICROSCOPE IMAGES

Yasuhiko Mori[1], Yoshihiko Obata[1], Shuichiro Nose[1]
P. Kriengsak[2] and Takateru Umeda[2]

[1]College of Industrial Technology, Nihon University, Chiba 275-8575, Japan
[2]Faculty of Engineering, The University of Tokyo, Tokyo 113-8656, Japan

ABSTRACT

In order to investigate the reason of low notch sensitivity in the strength of cast iron, tensile tests and acoustic emission measurements were conducted on the notched bar specimens of pearlitic spheroidal graphite cast iron. The fracture process occurred inside the material was reconstructed by the computer aided image processing for the topography of conjugate areas of the fracture surfaces observed by a confocal-optics-based scanning laser microscope. Reconstructed fracture process revealed that crack initiation and growth started in the middle of the specimen. Initial microcrack was created in the matrix around a graphite nodule. Acoustic emission onset load level, i.e., microfracture onset load level was approximately 90 % of the failure strength of the specimen, and the generation of acoustic emission was continuously observed until specimen rapture. As the load was increased, debonding occurred at the graphite/matrix interface, and coalesced with an initial microcrack to form a crack. Increasing load further caused slight growth of the crack in the matrix, and microcracks formation around the graphite nodules located near or ahead of the crack front. Thus, the crack growth in the specimen resulted from the repeated process of microcrack formation around the graphite nodule, growth, and coalescence to form a main crack. This study visually demonstrates that the graphite nodule acts as internal crack under the tri-axial stress state.

KEYWORD

fracture process, cast iron, notch effect, graphite, internal crack, scanning laser microscope

INTRODUCTION

It is known that the cast iron shows the low notch sensitivity in the strength [1]. The strength of the cast irons, however, depends on the sample shape or ductility of the materials. For instance, in the case of the bar specimen, it has been reported that the existence of notch had little influence on the strength [2] or on the contrary, increased the strength [3, 4]. Several models have been proposed for the explanation of this low notch sensitivity, such as the effect of the ununiformity of stress distribution around the notch root [3, 5, 6], or the internal notch effect of graphite nodule distributed in the matrix [7]. However, the detail of the fracture behavior occurred in the material has not been clarified. Therefore, the observation and analysis of the fracture process occurred inside the material is desired to give an answer for the reason of low notch sensitivity.

Kobayashi, et al. [8] has developed a fracture surface topography analysis technique, FRASTA, which combines a confocal-optics-based scanning laser microscope (SLM) and computer software to match three-dimensional features of conjugate fracture surfaces and reconstruct detailed fracture processes that occurred inside the material. Authors also have developed a technique, which can reconstruct the fracture process in microscopic detail, by using the computer aided image processing for the topography of conjugate fracture surfaces obtained by a SLM.

In the present paper, tensile tests and acoustic emission measurements were conducted on the bar specimens of pearlitic spheroidal graphite cast iron. SLM technique was applied for the broken sample to examine how the graphite nodules in the matrix contributed to the fracture process in the material. Actual dynamic fracture events occurred in the sample were estimated by the acoustic emission signals. This paper describes an attempt to seek an explanation for the reason of low notch sensitivity in the strength of the material tested and proposes a fracture model around the graphite nodule.

EXPERIMENTAL

The material used was a pearlitic spheroidal graphite cast iron, having retained pearlite of 98.9 %, nodularity of graphite of 81 %, graphite area of 9.5 %, graphite nodule per area of 244/mm^2, and mean graphite nodule of 22 micron.

Smooth bar with diameter of 6 mm and circumferentially notched bars with outer diameter of 10 mm were stressed and fractured in tensile. Shape of notches were U- and V-type, and these elastic stress concentration factor of notches, α, were evaluated to be 2.0 and 3.8, respectively.

Tensile test results showed that every type of specimens ruptured in rectangular fracture. Fracture strength (= tensile strength) of the smooth bar specimen was 940 MPa, showing the elongation of 6.6 %. Fracture strength of V-notched (α=3.8) specimen was 880 MPa. On the other hand, the sample failure of the U-notched specimen (α=2.0) occurred at a stress of 980 MPa, which exceeded the tensile strength of the smooth specimen by approximately 4 %.

Figure 1 shows the applied stress, σ, and the cumulative counts of AE events, N, as a function of elapsed time of tensile test, t, for the U-notched specimen. Stress applied increases continuously until the specimen rupture took place. Acoustic emissions start at stress level about 90 % of the fracture strength of the specimen and increase continuously until the specimen rupture.

Fracture surface analysis by using a scanning electron microscope (SEM) showed that in the case of the V-notched specimen, fracture initiated at the notch root. This resulted in the decrease in its strength from the strength of smooth specimen. In the case of U-notched specimen, however, the traces of crack initiation site were not clearly left on the fracture surface. So the fracture process occurred inside the U-notched specimen was reconstructed and analyzed by using SLM technique.

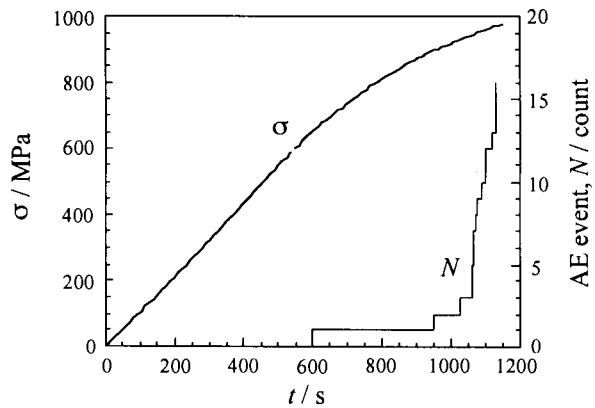

Figure 1: Applied stress, σ, and AE event counts, N, as a function of the testing time, t. U-notched specimen.

RECONSTRUCTION OF FRACTURE PROCESS

Figure 2 shows the macroscopic features of conjugate fracture surfaces of the U-notched sample. SLM observations were performed on the five locations on the conjugate surfaces, which are labeled I to V in Figure 2, because of the limitation of SLM field of view.

Figure 3 shows scanning-laser micrographs and corresponding gray-scale image topographs of conjugate fracture surfaces of the area location III in figure 2. Scanning-laser micrographs show that the graphite nodules are individually distributed in the matrix. Gray-scale images of the fracture topography of the conjugate fracture surfaces in the bottom of Figure 3 show that lighter areas are higher in elevation than darker areas.

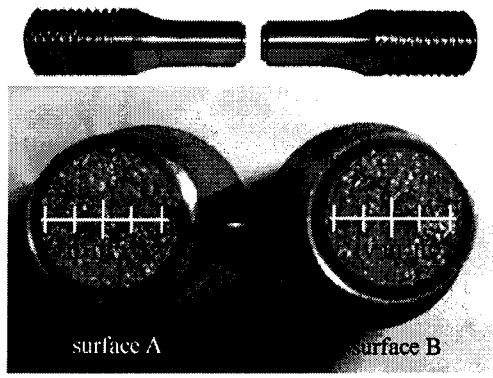

Figure 2: Macroscopic fracture surfaces of U-notched specimen broken in tensile.

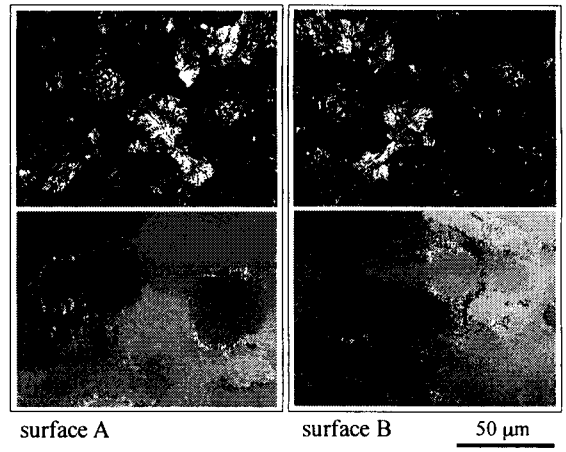

Figure 3: Scanning-laser micrographs, top, and corresponding topographs, bottom, of conjugate fracture surfaces of the location III in Figure 2.

The fracture process of this area was reconstructed using topographic information from Figure 3 (bottom) in digitized form. Maximum elevation resolution is 0.03 μm which is determined by dividing a specified range, i.e., the difference in elevation between the highest and lowest point within the observation field, by 256. Reconstruction of fracture process is accomplished by the following procedure. (1) Matching the three-dimensional features of conjugate fracture surfaces in a direction vertical to the specimen axis with the aid of a computer (Figure 4a through 4d). This makes a reference state (Figure 4d) for the successive procedure. If the surface irregularity, i.e., an elevation profile on the fracture surface is caused only by interaction of the crack tip with the microstructure and without inelastic deformation, the conjugate surface profiles should match precisely. Any mismatch appearing as overlap between the conjugate surface profiles indicates inelastic deformation (Figure 4d). (2) Separating the two surface irregularities from a

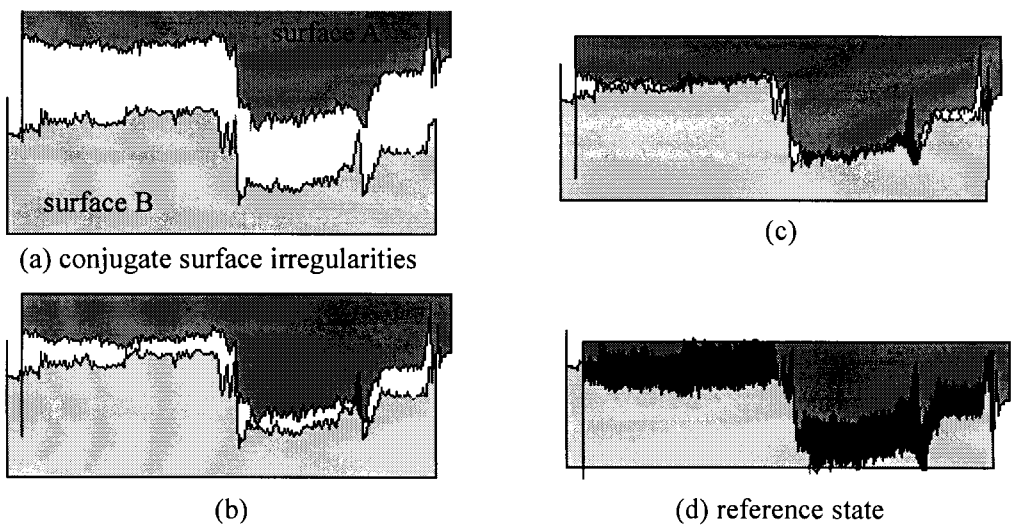

Figure 4: Procedure of fracture process reconstruction, showing conjugate surface irregularities in two-dimension. Matching process, (a) through (d); reconstruction of fracture process, (d) through (a).

matching reference state in a direction vertical to the specimen axis using computer software (Figure 4d through 4a). Displacement of the separation (ds) is increased step-by-step at a certain increment. Gaps, which appeared between the two surface irregularities in this sequential process, are projected on display equipment.

Figure 5 is a result of fracture process reconstructed for the location III shown in Figure 2, showing the step-by-step development of the fracture. Black areas, where the conjugate surface profiles overlap, denote intact material. White areas, where the surface profiles do not overlap, are considered locations where the fracture surfaces are separated, i.e., cracked. Projection diagrams of fractured areas show that cracking initiated in the matrix around graphite nodules (Figure 5a). As the applied stress is increased (see Figure 1), i.e., as the conjugate fracture surfaces are displaced relative to one another, as denoted as "ds" in Figure 5, microcracks grow slightly, debonding starts at the graphite/matrix interface (Figures 5b and 5c). Increasing the stress further causes coalescence of microcracks (Figure 5d) and development in the matrix forming a crack (Figure 5e).

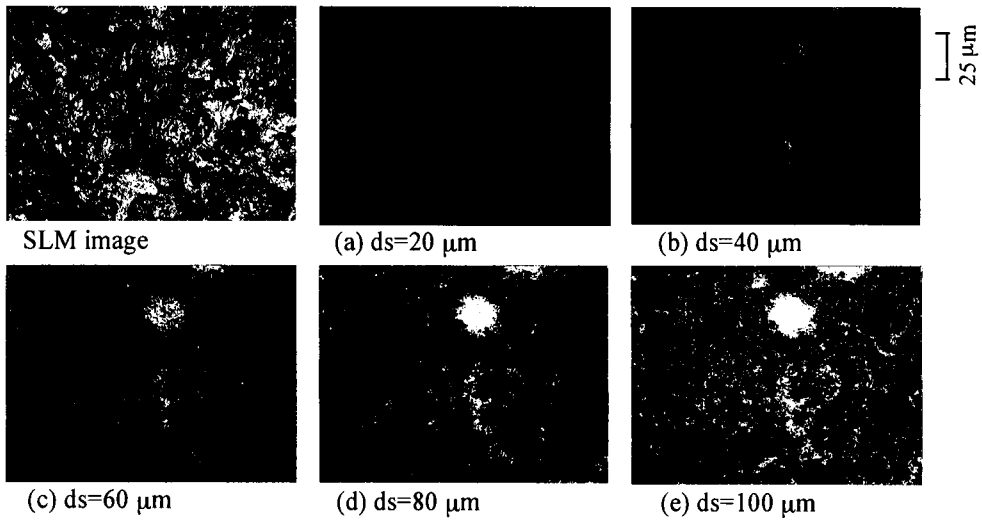

Figure 5: Scanning-laser micrograph, left top, and a series of projection diagrams of fractured areas, (a) to (e), of the location III shown in Figure 2.

In order to estimate the entire fracture process occurred in the specimen, fracture process for the locations I to V shown in Figure 2 were reconstructed with a same reference state. The reference state, that is, the state of the specimen before loading, was found in the location III, at which the matching of the conjugate surface profiles was completed. A series of fractured area projection diagrams in Figure 6 show the step-by-step development of the fracture. The reference state is the top of location III (center of the specimen) in the diagram. This result clearly demonstrates that as the stress is applied, microcrack initiates at around the graphite nodules distributed in the middle of the specimen (location III), as seen in Figure 5 in detail. With increasing the stress further, the microcracks are also created successively at the graphite nodules in the locations of II, I, IV and V. Then crack is formed by the coalescence of these microcracks and grows outward (toward the notch root of locations I or V), and specimen rupture takes place.

The displacement, ds, associates with the applied stress level, since the stress continuously increased until the specimen failure, as seen in Figure 1. In addition, acoustic emissions started at stress level about 90 % of the fracture strength of the specimen and increased continuously until the specimen rupture. Therefore, the fracture process shown in Figure 6 suggests for certain that crack initiation and growth started in the interior of the specimen. From the acoustic emission measurement, the nominal stress level of crack initiation was estimated to be approximately 850 MPa (Figure 1).

In this fracture process, the graphite nodule in the matrix behaves as void or pore in the typical ductile materials stressed in tensile. A model shown in Figure 7 could be proposed to explain the fracture process around the spheroidal graphite nodule. As the material (Figure 7a) is stressed in tensile and the stress reaches at a critical level, microcrack initiates in the part of matrix around graphite nodule (Figure 7b). Such Saturn's rings shape crack perpendicular to the stress axis could be created in the case, where the bonding between the graphite/matrix interface is not so rigid under the tri-axial stress state. As the stress

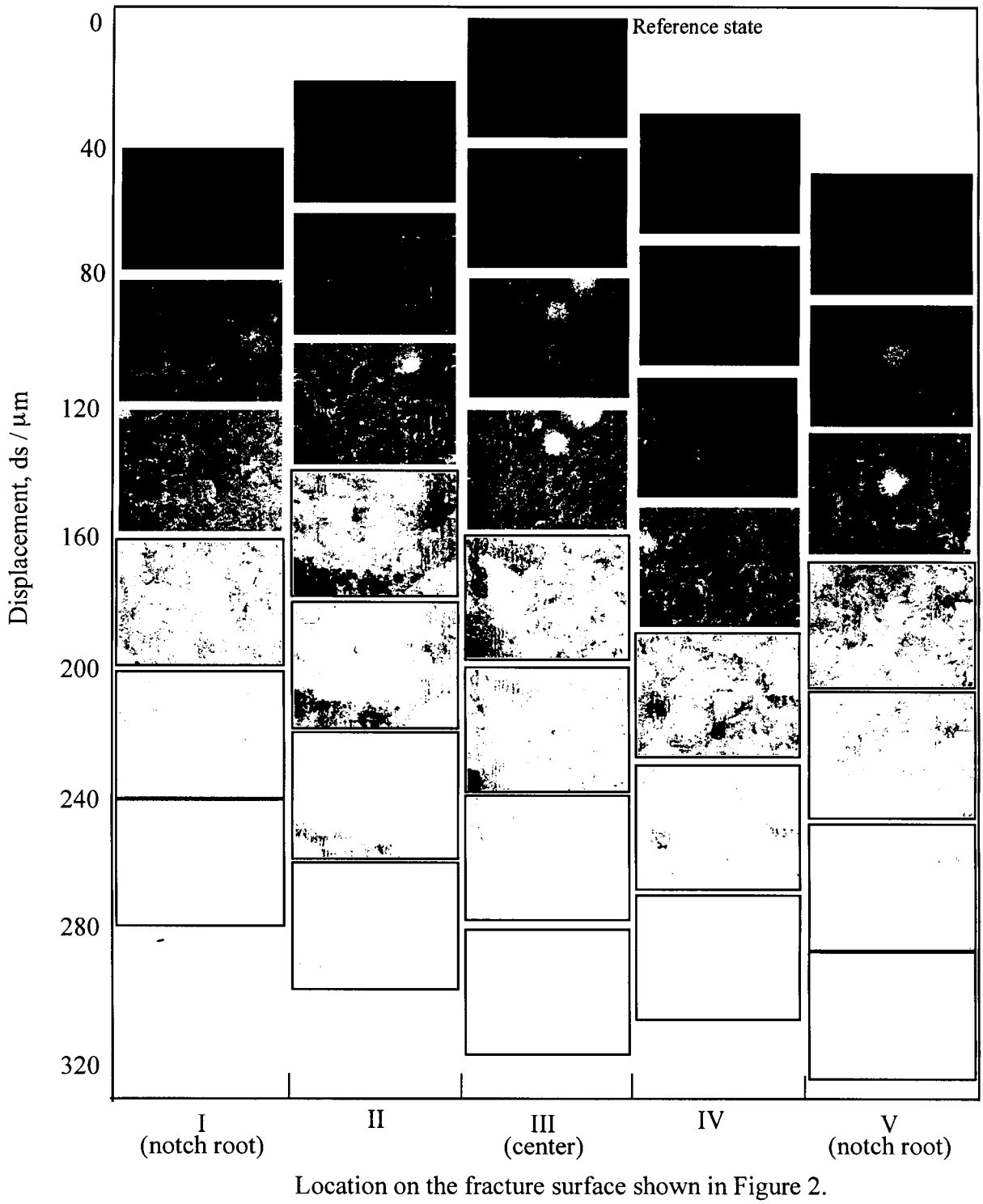

Figure 6: Fractured area projection diagrams for the locations I to V shown in Figure 2. Reconstructions of fracture process were performed with a same reference state.

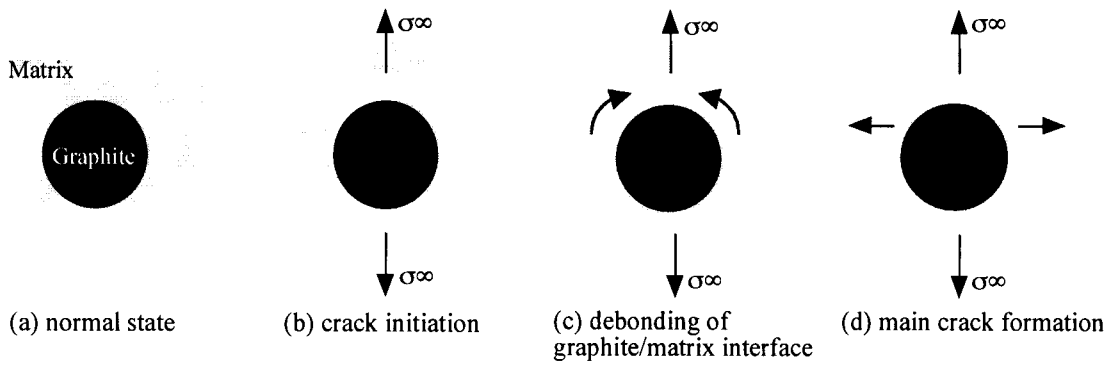

Figure 7: Model of fracture process occurred around the spheroidal graphite nodule.

is increased further, the debonding starts at the graphite/matrix interface, so that the ring shape crack merges into a crack (Figures 7c), then the crack grows into the matrix, forming a main crack (Figure 7d).

Cross sectional views of the fractured specimen observed by a scanning electron microscope are shown in Figure 8. Trace of the main crack shown in Figure 8a shows that the crack path twists around the surfaces of graphite nodules. Internal crack initiated from a graphite nodule, as shown in Figure 8b, is also found near the main crack path. These observations support the validity of the model proposed in Figure 7.

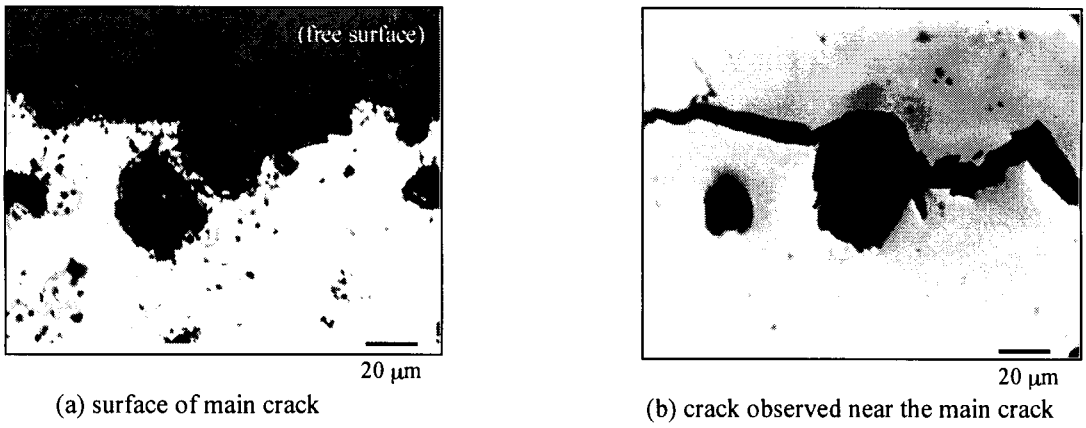

(a) surface of main crack

(b) crack observed near the main crack

Figure 8: Cross sectional views of the fractured sample.

SUMMARY

Regarding the reason of low notch sensitivity in the strength of cast iron, tensile tests and acoustic emission measurements were conducted on the notched bar specimens of pearlitic spheroidal graphite cast iron, and the fracture process occurred inside the material was reconstructed by the computer aided image processing for the topography of conjugate areas of the fracture surfaces observed by a confocal-optics-based scanning laser microscope.

Reconstructed fracture process revealed that crack initiation and growth started in the middle of the specimen. Initial microcrack was created in the matrix around a graphite nodule at a stress level of approximately 90 % of the specimen failure strength, which was estimated by the acoustic emission.

A model, which explains the fracture process occurred around the spheroidal graphite nodule under the tri-axial stress state, was proposed.

This study visually demonstrates that the graphite nodule acts as internal crack under the tri-axial stress state, and the strain energy release or redistribution of the internal stress due to this internal crack effect contributes to the elevation of the strength of notched specimen.

REFERENCES

1. A. F. S. (1957). *Cast Metal Handbook.* Des Plaines, Illinois, p. 92.
2. Nakanishi, F. and Okamoto, S. (1951). *Transaction of the Japan Society of Mechanical Engineering*, 17, 103.
3. Noguch, T. (1980). *J. The Society of Materials Science, Japan*, 29, 387.
4. Kriengsak, K., Satoh, K., Mori, Y., Paritud, B. and Umeda, T. (1995). *Proc. of the 3rd. Asian Foundry Congress*, pp. 296-303, The Korean Foundrymen's Society.
5. Noguchi, T. (1988). *Transaction of the Japan Society of Mechanical Engineering*, A, 54-507, 1962.
6. Takao and Nisitani. (1987). *J. The Society of Materials Science, Japan*, 36, 1060.
7. Ishibasi, T. (1952). *Transaction of the Japan Society of Mechanical Engineering*, 18, 87.
8. Kobayashi, T. and Shockey, D. A. (1987). *Metallurgical Transactions A*, 18A, 1941.